Available online at www.sciencedirect.com
SCIENCE DIRECT®
Journal of Sound and Vibration 270 (2004) 657–672
JOURNAL OF SOUND AND VIBRATION
www.elsevier.com/locate/jsvi

Torsional vibration suppression by wave-absorption control with imaginary system

Muneharu Saigo[a,*], Nobuo Tanaka[b], Dong Ho Nam[c,1]

[a] National Institute of Advanced Industrial Science and Technology, 1-2-1 Namiki, Tsukuba, Ibaraki 305-8564, Japan
[b] Tokyo Metropolitan Institute of Technology, 6-6 Asahigaoka, Hino, Tokyo 191-0065, Japan
[c] Incheon City College, Incheon, South Korea

Received 17 May 2002; accepted 4 February 2003

Abstract

We discuss vibration suppression in a lumped torsional system using wave-absorption control with online computation of an imaginary wave-propagation system similar to the real-controlled system. The basic concept of control was presented elsewhere for a multiple pendulum system to suppress free vibrations. We studied the suppression of forced vibration by a wave-absorption control for a lumped torsional system. Results confirmed that the proposed method works well on forced vibrations as on free vibrations. Initialization, setting amplitudes and velocities to zero, of the imaginary system for forced vibration control influences controlled amplitudes more than that for free vibration because vibration energy invariably comes in the system. Using numerical simulation, we studied initializations. Theoretical analysis on wave propagation in a lumped system has shown that smaller mass and larger spring stiffness of an imaginary system absorb vibration energy better, giving the optimum design for the imaginary system. Experiments are conducted for one-, two-, and three-degrees-of-freedom systems.

1. Introduction

Active vibration suppression in structures and mechanical systems consists primary of the modal vibration control and wave-absorption control. Modal vibration control is based on natural vibration modes, i.e., the system's standing-wave state. Wave-absorption control is based on vibration-energy absorption by impedance matching, i.e., the system's progressive-wave state. Modal vibration control is used widely in different fields, but wave-absorption control has

*Corresponding author.
E-mail address: m.saigo@aist.go.jp (M. Saigo).
[1] Currently with National Institute of Advanced Industrial Science and Technology, Japan.

0022-460X/03/$ - see front matter © 2003 Elsevier Science Ltd. All rights reserved.
doi:10.1016/S0022-460X(03)00185-8

advantages over modal vibration control in certain fields. The wave-absorption process is conducted based on local wave-propagation properties, with no need to deal with total system, and it is applicable to any system even if only information on the structure where waves propagate is known. Wave-absorption control, however, requires information on where waves propagate, making it suitable for one-dimensional (1-D) structures or assemblies of 1-D elements. Wave control in 1-D structures [1–9] has been widely studied. Von Flotow [1,2] and Miller and von Flotow [3] treated truss structures and power flow, and Fujii et al. [4,5] discussed design procedures for wave-absorption controllers with non-collocated sensors and actuators. Elliott and Billet [6] studied controllers with adaptive digital filters for beams, and Gardonio and Elliott [7] dealt with longitudinal and flexural waves in beams. Matsuda et al. [8] discussed a FEM-based transfer matrix approach, and Utsumi [9] presented analytical implementation of wave-absorption control for beams. The above studies dealt with continuous structures such as beams and truss structures. Wave propagation in periodic structures of lumped systems has long been treated [10], but wave-absorption control researches on lumped systems has been less so [11–13]. Examples include O'ccoure's [11] treatment of a lumped parameter mass-and-spring system as a model of a flexible arm and Saigo et al.'s [12,13] studies of a multiple-pendulums system. Another problem of wave-absorption control is that the control law includes the square root of Laplacian s, which cannot be implemented in real hardware by usual methods, meaning most studies in experiments have used approximations of the control law. To overcome this problem, we present a new method [12] that uses online computer simulation of a large degree-of-freedom (d.o.f) structural system having properties similar to the actual controlled system. This "imaginary" system is connected virtually to the real system by an actuator satisfying the continuity condition between real and imaginary systems, which we term wave-absorption control with an imaginary system (WCIS). WCIS realizes an infinite structural system free of wave reflections in the controlled real system if a suitable process is conducted to clear the vibrating energy in the imaginary system at appropriate timing. For this, WCIS initializes the imaginary system where deflections and velocities of all elements are set to zero except for the end element of the connecting side. Initialization should be done before the reflecting wave from the end of the imaginary system reaches the real system. In a previous study [12,13], we applied WCIS to free vibrations where total vibration energy is limited. It is not clear at this stage if WCIS is applicable to a general mechanical vibration system such as the mode-based vibration control strategy.

We apply WCIS to forced torsional vibration of multiple-d.o.f. system, studying the properties of initializations by numerical simulation. We studied wave propagation properties in a multiple-d.o.f. periodic system theoretically to obtain optimal parameters for the imaginary system, conducting experiments to confirm the effectiveness of WCIS.

2. Control law

2.1. Control strategy

The 1-D torsional vibration system considered consists of torsional bars and rigid discs (Fig. 1). Rigid lines represent the real system and dotted lines the imaginary system. Our control is to compensate for torque $k_{m+1}\phi_{m+1}$, i.e., generated at the (imaginary) connecting torsional bar

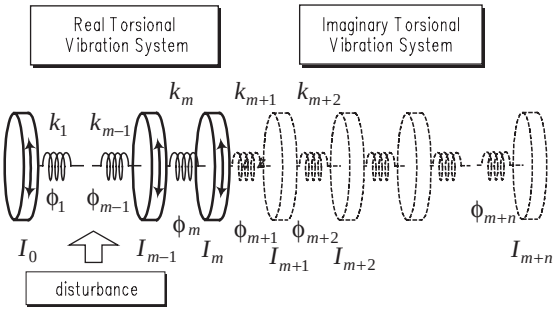

Fig. 1. Real and imaginary torsional vibration systems connected.

between the real and imaginary discs, by an actuator, and to absorb vibration energy in the real system propagated to the imaginary system. The imaginary system is assumed to have sufficient d.o.f. This process involves a quasi-infinite system and realizes nearly steady state wave propagation. The procedure is explained as follows by the use of the equation of motion:

Consider an $(m+n)$-d.o.f. torsional vibration system in which the controlled (real) system is m-d.o.f. and the imaginary system n-d.o.f. The equation of motion is expressed as

$$
\begin{aligned}
&\ddot{\phi}_1 + \frac{k_1}{I_{0,1}}\phi_1 - \frac{k_2}{I_1}\phi_2 = -\frac{T_0}{I_0},\\
&\vdots\\
&\ddot{\phi}_m - \frac{k_{m-1}}{I_{m-1}}\phi_{m-1} + \frac{k_m}{I_{m-1,m}}\phi_m \boxed{- \frac{k_{m+1}}{I_m}\phi_{m+1}} = -\frac{T_{m-1}}{I_{m-1}} + \frac{T_m}{I_m},\\
&\ddot{\phi}_{m+1} - \frac{k_m}{I_m}\phi_m + \frac{k_{m+1}}{I_{m,m+1}}\phi_{m+1} - \frac{k_{m+2}}{I_{m+1}}\phi_{m+2} = 0,\\
&\vdots\\
&\ddot{\phi}_{m+n} - \frac{k_{m+n-1}}{I_{m+n-1}}\phi_{m+n-1} + \frac{k_{m+n}}{I_{m+n-1,m+n}}\phi_{m+n} = 0,\\
&\frac{1}{I_{i,j}} \equiv \frac{1}{I_i} + \frac{1}{I_j},
\end{aligned}
\tag{1}
$$

where k_i, I_i, ϕ_i are the spring constant of ith torsional bar, the moment of inertia of ith rigid disc, and the torsional angle of ith torsional bar. External disturbance on the ith disc is expressed as T_i. The moment of inertia of the left-end disc and the external disturbance on it are represented by I_0 and T_0.

The vibration energy in the real system propagates to the imaginary system based on propagation properties when Eq. (1) is completely realized. Elements whose suffixes exceed $(m+1)$ in Eq. (1) are virtual, so, we must compensate for the term relating to ϕ_{m+1} (enclosed by a solid rectangle in Eq. (1)) as control acceleration. Equations of motion including variables whose suffixes exceed $(m+1)$ are solved by online calculation, where variable ϕ_m (enclosed by a dot–dash rectangle in Eq. (1)) is measured. This process is a feedforward control

with a single input and single output because the measured variable ϕ_m is not compensated for directly.

The above control strategy is based on the concept that the wave-absorption control is equivalent to making the controlled system having no wave reflections at the boundary, i.e., to virtually realize an infinite structure in a finite structure. Our control strategy to connect a virtually large-d.o.f. system with initialization detailed in the section below is wave-absorption control, even though the control strategy does not use wave-absorption conditions as in wave control of elastic continuous structures in Refs. [1–9].

2.2. Initialization of imaginary system

In an insufficient-d.o.f. imaginary system for total energy to be absorbed, the imaginary system must have no kinetic and potential energy, with initialization of the imaginary system, at appropriate timing. We use [12,13] the following initialization; when $\phi_m = 0$ or $\dot{\phi}_m = 0$, all imaginary variables are set to zero, $\phi_{m+i} = \dot{\phi}_{m+i} = 0$ ($i = 1$ to n), which we term RDI′ and RVI′. These initializing timings are considered to influence the real system less because no energy or energy flow exists in the connecting spring k_m at this moment. The continuity of $\dot{\phi}_{m+1}$ in RDI′ and ϕ_{m+1} in RVI′ may enhance control performance, termed RDI and RVI. RDI sets $\phi_{m+1} = \phi_{m+i} = \dot{\phi}_{m+i} = 0$ ($i = 2$ to n) when $\phi_m = 0$ and keeps $\dot{\phi}_{m+1}$ unchanged, and RVI sets $\phi_{m+i} = \dot{\phi}_{m+1} = \dot{\phi}_{m+i} = 0$ ($i = 2$ to n) when $\dot{\phi}_m = 0$ and keeps ϕ_{m+1} unchanged. These are tried for the first time, to our knowledge, in this paper. The above four methods initializing at $\phi_m = 0$ or $\dot{\phi}_m = 0$, RDI′, RVI′, RDI and RVI (R-methods), are modified to IDI′, IVI′, IDI, and IVI (I-methods) initializing at $\phi_{m+1} = 0$ or $\dot{\phi}_{m+1} = 0$. R-methods are based on the vibration state of the real system and I-methods on the imaginary system. In diagrammed R-methods (Fig. 2), initialization is conducted at each timing of $\phi_m = 0$ or $\dot{\phi}_m = 0$. It is sufficient to initialize system after condition $|\phi_{m+n}| \geqslant \varepsilon$ is satisfied, where positive value ε is given appropriately. Reducing the number of initializations per unit time diminishes the undesirable influence of initialization on the real system, but it is difficult to get optimum ε theoretically because it depends on the vibration state of the system.

2.3. Optimization of imaginary systems

To obtain optimal parameters of the imaginary system as a vibration energy absorber, we analyzed a periodic disc-and-torsional spring system theoretically. The kth equation of motion of the system (Fig. 3) is

$$\ddot{\phi}_{k+1} - \frac{k}{I}\phi_k + 2\frac{k}{I}\phi_{k+1} - \frac{k}{I}\phi_{k+2} = 0 \quad (k \neq 1, 0). \tag{2}$$

Laplace transformation of Eq. (2) is

$$\mathbf{\Phi}_{k+2}(s) - \left(2 + \frac{I}{k}s^2\right)\mathbf{\Phi}_{k+1}(s) + \mathbf{\Phi}_k(s) = 0, \tag{3}$$

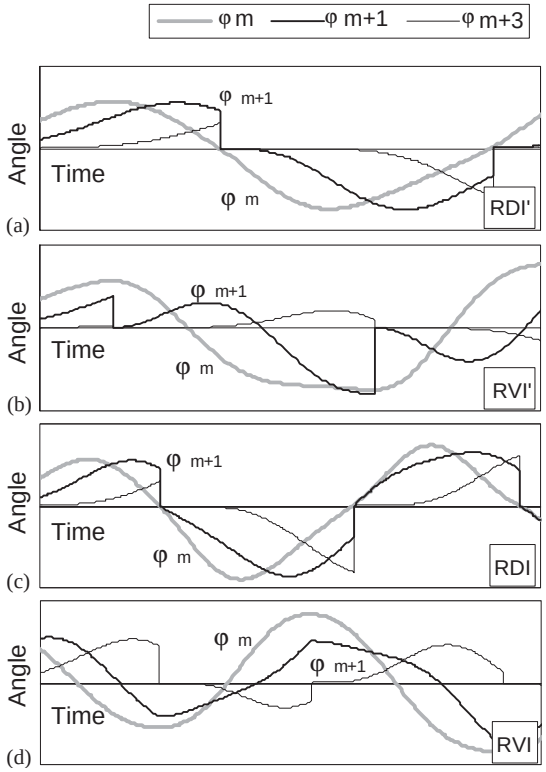

Fig. 2. Initialization of R-type for m-d.o.f. real and n-d.o.f. imaginary systems, (a) RDI′: $\phi_{m+i} = \dot{\phi}_{m+i} = 0$ ($i = 1$ to n) at $\phi_m = 0$, (b) RVI′: $\phi_{m+i} = \dot{\phi}_{m+i} = 0$ ($i = 1$ to n) at $\dot{\phi}_m = 0$, (c) RDI: $\phi_{m+1} = \phi_{m+i} = \dot{\phi}_{m+i} = 0$ ($i = 2$ to n) at $\phi_m = 0$, (d) RVI: $\dot{\phi}_{m+1} = \phi_{m+i} = \dot{\phi}_{m+i} = 0$ ($i = 2$ to n) at $\dot{\phi}_m = 0$.

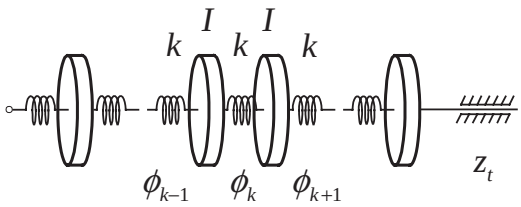

Fig. 3. Homogenous disc and torsional spring system with terminal impedance.

where $\mathbf{\Phi}_k(s)$ is Laplace transformation of ϕ_k. Substituting general solution $\mathbf{\Phi}_k(s) = \beta^k$ into Eq. (3), we obtain the specific roots

$$\beta = 1 + s^2 \frac{I}{2k} \mp \sqrt{\left(1 + s^2 \frac{I}{2k}\right)^2 - 1} \equiv 1 + s^2 \frac{I}{2k} \mp \sqrt{\beta^0} \equiv \beta^+, \beta^- \tag{4}$$

and the general solution

$$\mathbf{\Phi}_k(s) = c_1(s)(\beta^+)^k + c_2(s)(\beta^-)^k \equiv \mathbf{\Phi}_k^+(s) + \mathbf{\Phi}_k^-(s), \tag{5}$$

where $c_1(s)$and $c_2(s)$ are arbitrary constants determined by boundary conditions.

When β^0 in Eq. (4) is negative, β^+ represents a positive propagating solution and β^- a negative propagating solution. By introducing $s = \mathrm{j}\omega$ (j is the imaginary unit), the condition of existence of propagating solution $\beta^0 \leqslant 0$ gives the limit frequency as

$$\omega \leqslant 2\sqrt{k/I} \equiv 2\,\omega_0. \tag{6}$$

The mechanical impedance for the positive propagating solution is

$$z^+(s) = \frac{s}{k(1-\beta^+)}. \tag{7}$$

When terminal impedance z_t is $z^+(s)$, no wave reflection occurs.

The no wave reflection above is ideal as a wave absorber and expressed in mobility form as

$$\lambda = \frac{k}{\omega_0}\left\{\sqrt{1-\frac{1}{4}\left(\frac{\omega}{\omega_0}\right)^2} - \mathrm{j}\frac{\omega}{2\omega_0}\right\}. \tag{8}$$

Eq. (6) shows that the disc-and-torsional spring wave absorber must have a specific frequency $\omega_0 = \sqrt{k/I}$, i.e., greater than half of the disturbance frequency of the controlled system. Eq. (8) shows that a larger spring constant better absorbs the vibration energy for a given input velocity and a specific frequency.

From Eq. (4), we obtain

$$|\beta^{+(-)}|^2 = 1, \tag{9}$$

which means the steady state wave amplitude is constant regardless of the frequency. The wave propagation condition thus realizes no resonance occurring in the standing-wave condition, but antiresonance phenomena simultaneously disappear. The amplitude of the wave propagation condition near the frequency of antiresonance occurring in a standing-wave condition may exceed that of uncontrolled amplitude, although these amplitudes are very small.

The phase difference between two adjacent elements in a wave propagation condition is obtained by substituting $s = \mathrm{j}\omega(= \mathrm{j}\nu\omega_0)$ to β^+ of Eq. (4) (Fig. 4). Eq. (9) and Fig. 4 evidence the wave propagation condition of a vibrating system.

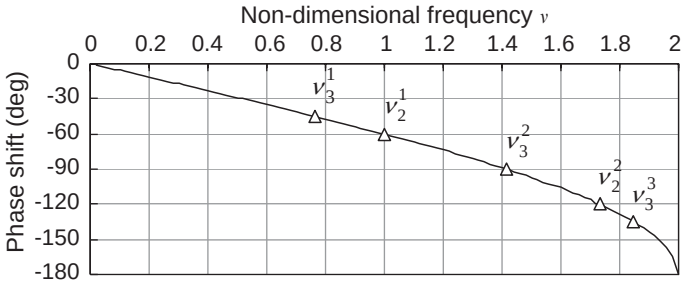

Fig. 4. Phase difference in torsional angle between adjacent elements, ν_i^j: Non-dimensional resonance frequency (i: number of d.o.f., j: number of mode; $\nu_2^1 = 1.0$, $\nu_2^2 = 1.73$, $\nu_3^1 = 0.765$, $\nu_3^2 = 1.41$, $\nu_3^3 = 1.85$).

3. Simulation

3.1. Homogeneous real system

Here, we treat a three-d.o.f. homogeneous real system where all torsional springs and discs are the same. Parameters of the analytical real system are the same as those of the experiment detailed in the next section, the moment of inertia $I = 0.0123\,\mathrm{kg\,m^2}$, and spring constant of torsional bar $k = 21.4\,\mathrm{N\,m}$. Parameters of the imaginary system are the same as for the real system except for the number of d.o.f. Disturbance torque T_0 is applied to the left end disc of the real system.

Fig. 5 shows the controlled response using the 40-d.o.f. imaginary system calculated by the sampling period of 1 ms and IVI initialization. The time when variable ϕ_{43} ($m = 3, n = 40$) is set to zero is the initializing timing. Disturbance acceleration T_0/I is $\sin(v\omega_0 t)(\omega_0 = \sqrt{k/I};\ v = 0.566)$. Note the influence of initialization seen just after the initialization timing as the larger amplitude. Virtually no influence is observed, however, after 1 period of disturbance. Fig. 6 shows the controlled amplitude versus disturbance frequency with a 40-d.o.f. imaginary system and IDI′ initialization. △ denotes the steady state amplitude in which the influence of initialization died away, and ◇ the maximum amplitude just after initialization. Steady state amplitudes are constant below the wave propagation limit frequency given by Eq. (6), which coincides with the analytical result Eq. (9). These steady state amplitudes coincide with those of a sufficiently large-d.o.f. system obtained by modal vibration analysis with nearly zero frequency disturbance, not with those of a three-d.o.f. system (Fig. 6).

Figs. 7 shows the timing chart at resonance frequencies. Control starts 2 s after disturbance is applied. These are typical features of wave control; after control starts, all amplitudes propagate with the same magnitude and constant phase shift through a transient period. We compare the phase difference in wave propagation state between ϕ_1 and ϕ_3 (Fig. 7) and the theoretical states (Fig. 4). The theoretical phase shift between adjacent elements at frequencies $v = 0.765$ (first-resonance frequency), 1.41 (second-resonance frequency) and 1.85 (third-resonance frequency) are $-45°$, $-90°$ and $-135°$. Note the phase difference between ϕ_1 and ϕ_3 is about $2\times(-45)°$, $2\times(-90)°$ and $2\times(-135)°$, coinciding with the theoretical ones. The theoretical results (4) and (9) are thus key features of the wave propagation condition of the homogeneous system.

We have presented 8 types of initialization —RDI, RDI′, RVI, RVI′, IDI, IDI′, IVI, and IVI′. We found no general qualitative tendency among these methods by simulations, however, because

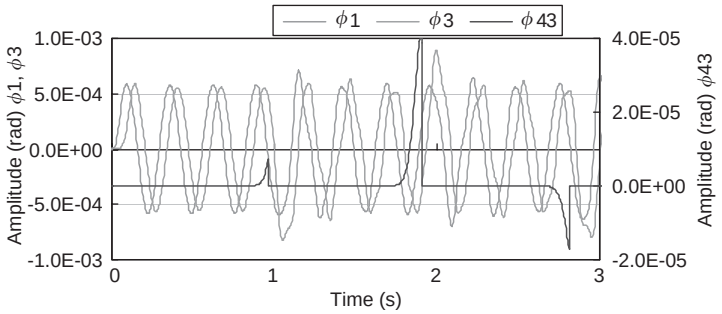

Fig. 5. Influence of initialization on three-d.o.f. real system with 40-d.o.f. imaginary system, IVI initialization, and non-dimensional disturbance frequency $v = 0.566$.

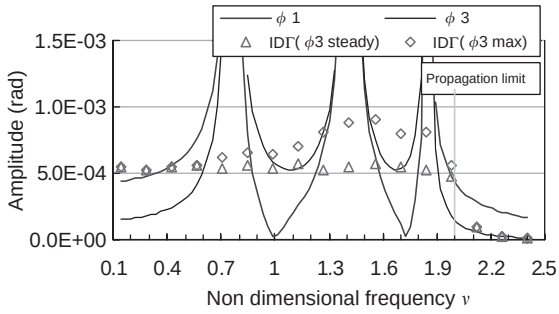

Fig. 6. Calculated response of three-d.o.f. real system to disturbance sin $v\omega_0 t$ using 40-d.o.f. imaginary system and IDI' initialization, —— steady state amplitude of ϕ_1 by modal vibration analysis, —— steady state amplitude of ϕ_3 by modal vibration analysis, △ steady state amplitude of ϕ_3 by wave control, ◇ maximum amplutide of ϕ_3 just after initialization by wave control.

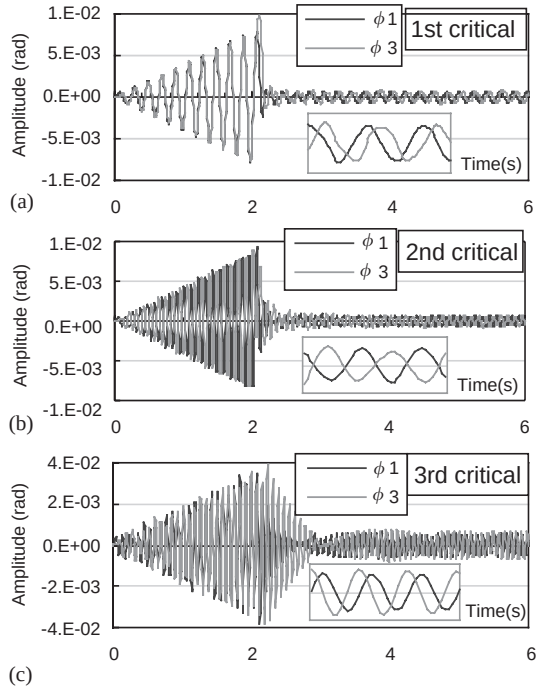

Fig. 7. Response by control starting 2 s of three-d.o.f. real system at resonance speeds with 40-d.o.f. imaginary system and IVI′ initialization at (a) first-resonance speed $v = 0.765$, (b) sencond resonance speed $v = 1.41$, and (c) third resonance speed $v = 1.85$.

controlled amplitudes depend on computation conditions such as initial conditions, ε detailed in Section 2.2, and the number of d.o.f. of real and imaginary systems. We cannot yet conclude which method is best. Below, we show results of I-methods as examples. Fig. 8 shows maximum amplitudes versus disturbance frequency for 10-d.o.f. and 40-d.o.f. imaginary systems. Maximum amplitudes depend significantly on the disturbance frequency and the smaller d.o.f. imaginary

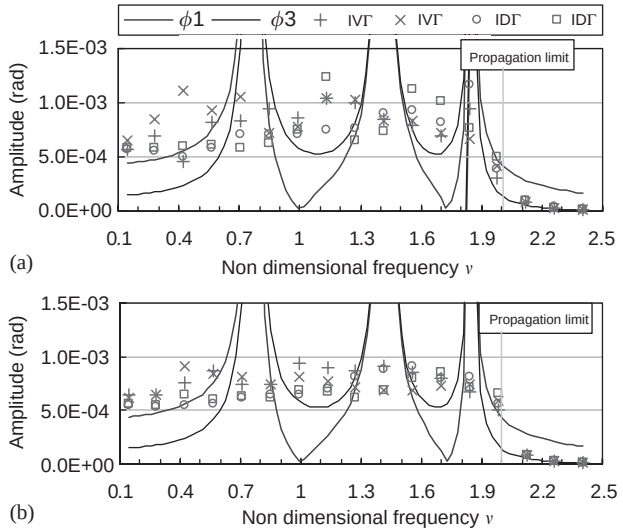

Fig. 8. Maximum response of ϕ_3 by wave control with (a) 10-d.o.f. and (b) 40-d.o.f. imaginary systems, —— steady state amplitude of ϕ_1 by modal vibration analysis, —— steady state amplitude of ϕ_3 by modal vibration analysis.

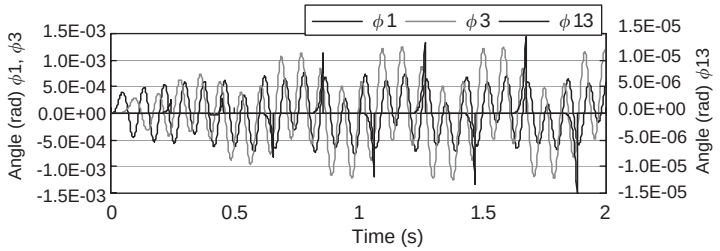

Fig. 9. Influence of initialization on small imaginary sytem for 10-d.o.f. imaginary system, IDI′ initialization and non-dimensional disturbance frequency $\nu = 1.84$.

system has worse performance. Frequent initialization due to the smallness of the imaginary system does not give a steady state condition such as seen in Fig. 5. Fig. 9 shows a typical example in which low-frequency vibration arises synchronized with initialization timing in addition to disturbance frequency vibration. Initialization occurs before steady state vibration is established. Comparing Figs. 8(a) and (b), the 40-d.o.f. imaginary system shows better performance in initialization than the 10-d.o.f. imaginary system, so, the best way to avoid the undesirable influence of initialization is to use a large-d.o.f. imaginary system.

3.2. Non-homogeneous real systems

We discuss control performance of WCIS for non-homogeneous three-d.o.f. real systems using a homogeneous imaginary system. The disc-and-torsional spring imaginary system absorbs vibration energy if condition (6) is satisfied. This condition is realized for arbitrary disturbance

Table 1
Parameters used in Fig. 8

Case	Spring constant	Non-dimensional first critical frequency (κ)		Non-dimensional second critical frequency (κ)		Non-dimensional third critical frequency (κ)	
A	$k_1 = 20$, $k_2 = 10$, $k_3 = 1$	1.12	(1,5,15)	3.66	(5,10,15)	6.88	(15,20,30)
B	$k_1 = 10$, $k_2 = 20$, $k_3 = 1$	1.13	(1,5,15)	3.61	(5,10,15)	6.9	(15,20,30)
C	$k_1 = 0.05$, $k_2 = 0.1$, $k_3 = 1$	0.223	(1,5,15)	0.443	(1,5,15)	1.43	(1,5,15)
D	$k_1 = 0.1$, $k_2 = 0.05$, $k_3 = 1$	0.207	(0.1,1,10)	0.24	(1,10)	1.42	(1,10,20)
E	$k_1 = 20$, $k_2 = 0.05$, $k_3 = 1$	0.222	(0.1,1,20)	1.42	(1,10,20)	6.33	(10)
F	$k_1 = 0.05$, $k_2 = 20$, $k_3 = 1$	0.257	(1,10)	1.22	(1,5,10)	6.37	(15,30,45)

Resonance frequency $= v_i\sqrt{k_3/I}$.

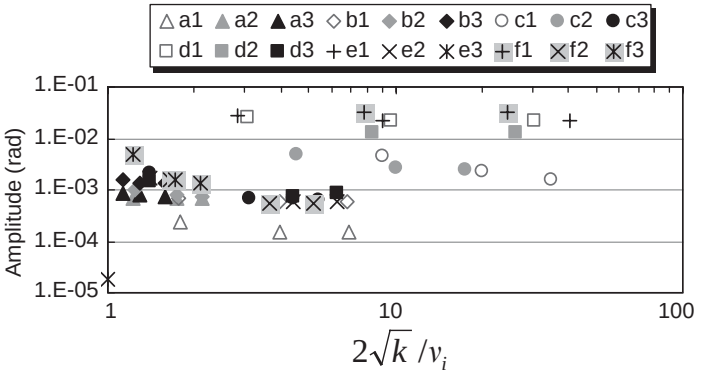

Fig. 10. Response of non-homogeneous real system at resonance frequencies, symbol α i: case α(=a,b,c,d,e,f) and number of mode i, v_i: non-dimensional resonance frequency in Table 1, κ: parameter in Table 1.

frequency by using a large enough spring constant. If the amplitude of the element adjacent to the imaginary system is extremely small compared to those of other elements, however, controlled amplitudes of some elements may increase. This property is based on mode shapes of the resonance of real system. We analyze six cases of a spring constant, i.e., six different resonance mode shapes (Table 1): (a) $k_1 : k_2 : k_3 = 20 : 10 : 1$; (b) $k_1 : k_2 : k_3 = 10 : 20 : 1$; (c) $k_1 : k_2 : k_3 = 0.05 : 0.1 : 1$; (d) $k_1 : k_2 : k_3 = 0.1 : 0.05 : 1$; (e) $k_1 : k_2 : k_3 = 20 : 0.05 : 1$; and (f) $k_1 : k_2 : k_3 = 0.05 : 20 : 1$. The imaginary system has spring constant $\kappa \times k_3$, where κ is a parameter. The moment of disc inertia is the same as the experimental one in both real and imaginary systems, and k_3 is fixed as the experimental one. Disturbance acceleration $\sin(v_i\sqrt{k_3/I}t)$ is applied to the disc I_3, where v_i is the non-dimensional ith resonance frequency. Fig. 10 shows the maximum amplitudes among three elements at each resonance frequency obtained by the 40-d.o.f. imaginary

system and IDI′ initialization. The axis of abscissa $2\sqrt{\kappa}/v_i$ represents the ratio on the right side of Eq. (6), $2\sqrt{\kappa k_3/I}$, to the left side of Eq. (6), $v_i\sqrt{k_3/I}$, and corresponds to the margin of resonance frequency from the wave propagation limit. The propagation limit is represented as $2\sqrt{\kappa}/v_i = 1$. The same symbols in Fig. 10 show the effect of κ on the controlled amplitude of each resonance frequency. Some resonance frequencies have amplitudes that are quite large, e.g., exceeding 1.0E-2, and do not decrease as κ becomes larger; d1:case (d) 1st critical, e1:case (e) 1st critical, f1:case (f) 1st critical, d2:case (d) 2nd critical, etc. Natural resonance modes of these cases have very small amplitudes of ϕ_3, and the energy absorbed by the imaginary system is quite small compared to total vibration energy. Based on this, we say that the wave control performance of non-homogeneous systems depends on natural vibration modes, not on the disturbance frequency, and is not substantially changed by the design of the imaginary system.

4. Experiments

Fig. 11 shows the experimental apparatus. The homogeneous real vibration system consists of discs 200 mm in diameter and 20 mm thick and torsional bars 4 mm in diameter and 100 mm long for two- and three-d.o.f. systems and 210 mm long for one-d.o.f. system. AC servomotors are used for drive and control. The drive motor has a rated torque of 0.9 N m and a rated speed of 3000 r.p.m. and the control motor has a rated torque of 0.16 N m and a rated speed of 3000 r.p.m. The measurement system consists of rotary encoders, a torsional angel converter, low-pass and high-pass filters, and a personal computer (CPU clock: 266 MHz). Torque disturbance is applied by torque fluctuation of the AC drive motor in constant speed mode, which is 4 times, 2 times, and 1 time per rotation, so, resonance may occur at a rotation speed of $\frac{1}{4}$, $\frac{1}{2}$, and $\frac{1}{1}$ of the natural frequency. Torque magnitude cannot be adjusted. A 10-d.o.f. imaginary system is computed by the Euler method with a sampling period of 3 ms. Experiments are conducted for one-, two-, and three-d.o.f. with the same control program.

Fig. 12 shows controlled and uncontrolled amplitudes at the first-resonance frequency of the two-d.o.f. real system, where control starts at about 0.8 s (the computer and the recorder are not linked). Fig. 12(a) shows amplitudes of ϕ_1 and ϕ_2. Figs. 12(b) and (c) show ϕ_1 and $2\,\phi_2$.

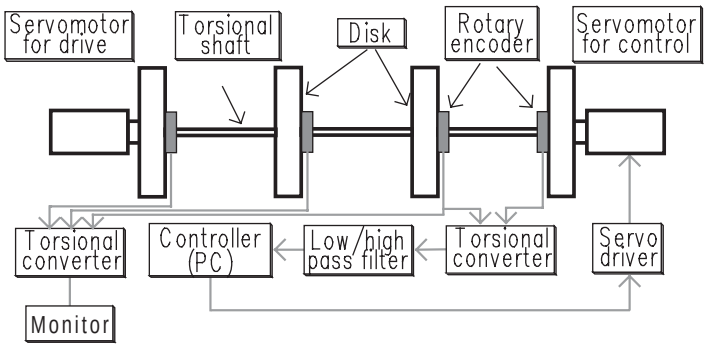

Fig. 11. Experimental apparatus.

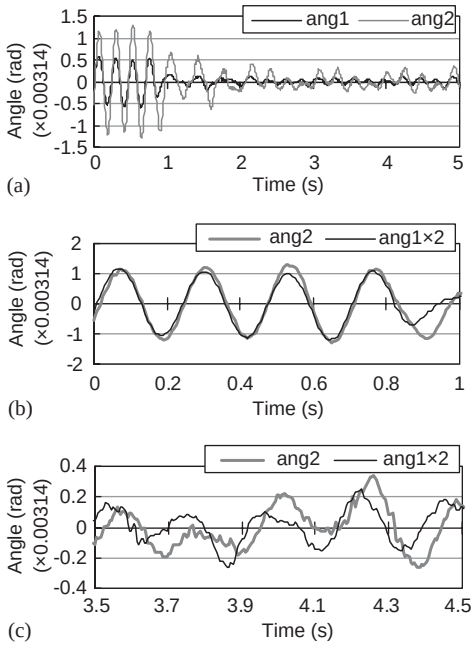

Fig. 12. Experimental waveforms of two-d.o.f. real system at 4.32 Hz excitation. (first-mode resonance); ang1: ϕ_1, ang2: ϕ_2.

Figs. 12(b) and (c) show amplitudes on the magnified time scale. Amplitudes are suppressed considerably by control and the phase between ϕ_1 and ϕ_2 of the controlled amplitudes is shifted (Fig. 12(c)). The non-dimensional frequency of the first torsional resonance of the two-d.o.f. real system v_2^1 is 1, and the corresponding theoretical phase shift is -60° (Fig. 4). Fig. 12(c) shows the phase difference between ϕ_1 and ϕ_2 is about -60°. The correspondence of phase shifts between experimental and theoretical results shows that wave control is realized in the experimental set-up. Fig. 13 shows uncontrolled and controlled amplitudes at the second-resonance frequency of the two-d.o.f. real system and the correspondence of phase shifts between experimental and theoretical results similar to the first-resonance case.

Fig. 14 shows experimental results for the one-d.o.f. real system with RDI′ initialization. Resonance occurs at 1.1, 2.2, and 4.4 r.p.s. when uncontrolled, and the effect of vibration suppression by control is marked at these resonance speeds. Fig. 15 shows experimental results for the two-d.o.f. real system with RDI′ initialization. Resonance occurs at 0.92 and 4.3 r.p.s. of the first-mode resonance, and 1.81 and 3.62 r.p.s. of the second-mode resonance when uncontrolled. At these resonance speeds, vibration amplitudes are remarkably suppressed by control. Fig. 16 shows experimental results for the three-d.o.f. real system with RVI′ initialization. Resonance occurs at 0.84 and 3.37 r.p.s. of the first-mode resonance, 1.48 and 5.9 r.p.s. of the second-mode resonance, and 3.86 and 7.72 r.p.s. of the third-mode resonance. In this case, control is somewhat worse than for one- and two-d.o.f. systems. Figs. 17(a)–(d) show the timing charts of the three-d.o.f. case at 0.84 and 3.37 r.p.s. of the first-mode resonance, 5.9 r.p.s. of the second-mode resonance, and 7.72 r.p.s. of the third-mode resonance. Figs. 17(a) and (d) show vibrations of low frequency besides those of torque-induced frequency such in Fig. 9. If we ignore these

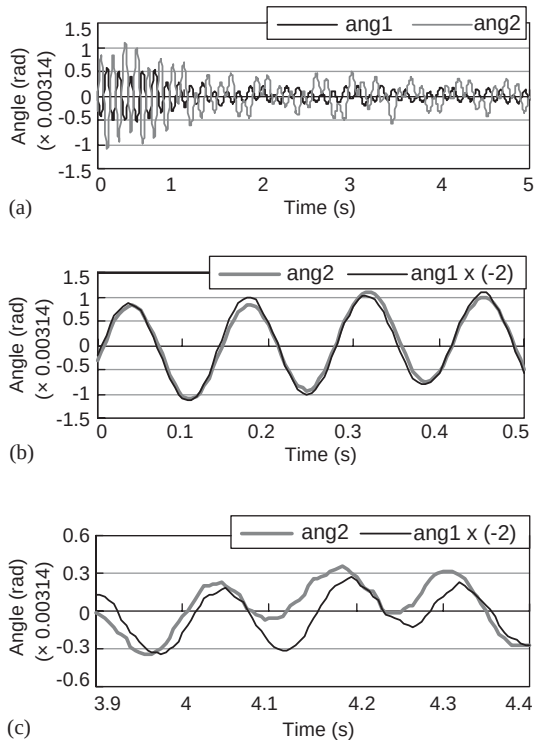

Fig. 13. Experimental waveforms of two-d.o.f. real system at 7.24 Hz excitation (second-mode resonance); ang1: ϕ_1, ang2: ϕ_2.

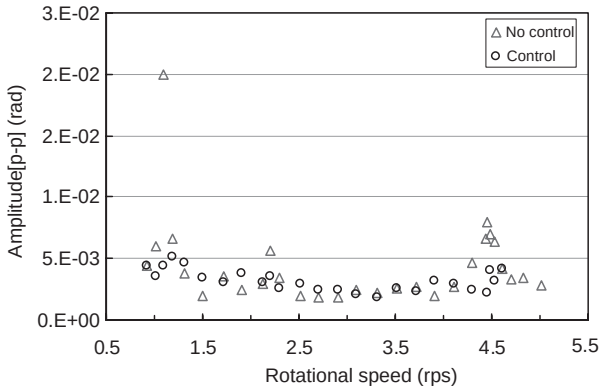

Fig. 14. Experimental response ϕ_1 of one-d.o.f. real system.

low-frequency vibrations, controlled amplitudes in Fig. 17 are nearly the same level as in one- and two-d.o.f. systems.

Our experimental apparatus is not perfect for WCIS, but experimental results show that it is easy to realize WCIS for forced vibration.

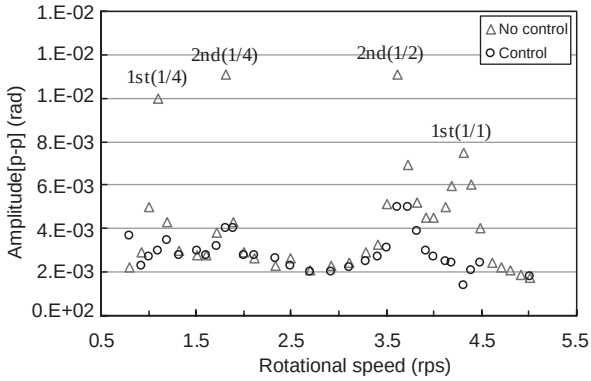

Fig. 15. Experimental response ϕ_2 of two-d.o.f. real system.

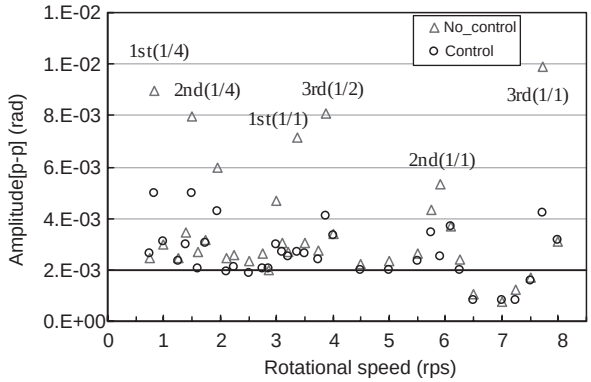

Fig. 16. Experimental response ϕ_3 of three-d.o.f. real system.

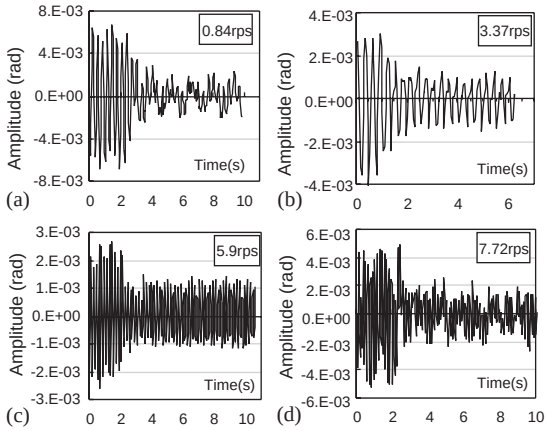

Fig. 17. Timing chart of three-d.o.f. real system experiment at a speed of (a) a quarter of first resonance, (b) first resonance, (c) second resonance, and (d) third resonance.

5. Conclusions

We have shown by simulation and experiment the effectiveness of wave absorption control with an imaginary system in suppressing torsional forced vibration. Our major results are as follows:

(1) Wave-absorption control is possible in a 1-D multiple-d.o.f. torsional forced vibration system by connecting the imaginary and real systems and compensating for connection torque.
(2) The optimum design of an imaginary system consisting of discs and torsional springs has a large specific frequency and a large spring constant.
(3) A larger d.o.f. imaginary system reduces undesirable effects of initialization more than a smaller d.o.f. imaginary system.
(4) Wave control with the imaginary system is effective for a real system having large vibration amplitudes of the connection element when uncontrolled, so, control performance depends on natural resonance modes for non-homogeneous real systems.

Appendix A. Nomenclature

k_i, k spring constant of ith torsional bar for non-homogeneous and homogeneous systems
I_i, I moment of inertia of ith disc for non-homogeneous and homogeneous systems
ϕ_i angle of ith torsional bar
T_i disturbance torque on ith disc
ω_0 specific frequency for homogeneous system ($= \sqrt{k/I}$)
v non-dimensional frequency normalized by ω_0
v_i^j non-dimensional jth resonance frequency of i-d.o.f. system normalized by ω_0
t time

References

[1] A.H. von Flotow, Traveling wave control for large spacecraft structures, Journal of Guidance, Control, and Dynamics 9 (4) (1986) 462–468.
[2] A.H. von Flotow, Disturbance propagation in structural networks, Journal of Sound and Vibration 106 (3) (1986) 433–450.
[3] D.W. Miller, A. von Flotow, A traveling wave approach to power flow in structural networks, Journal of Sound and Vibration 128 (1) (1989) 145–162.
[4] H. Fujii, T. Ohtsuka, T. Murayama, Wave absorbing control for flexible structures with noncollocated sensors and actuators, Journal of Guidance, Control, and Dynamics 15 (2) (1992) 431–439.
[5] H. Fujii, T. Ohtsuka, Experiment of a noncollocated controller for wave cancellation, Journal of Guidance, Control, and Dynamics 15 (3) (1992) 741–745.
[6] S.J. Elliott, L. Billet, Adaptive control of flexural waves propagating in a beam, Journal of Sound and Vibration 163 (2) (1993) 295–310.
[7] P. Gardonio, S.J. Elliott, Active control of waves on a one-dimensional structure with a scattering termination, Journal of Sound and Vibration 192 (3) (1996) 701–730.
[8] K. Matsuda, Y. Kanemitsu, S. Kijimoto, A wave-based controller design for general flexible structures, Journal of Sound and Vibration 216 (2) (1998) 269–279.

[9] M. Utsumi, Analytical implementation of wave-absorbing control for flexible beams using synchronization condition, American Society of Mechanical Engineers, Journal of Vibration and Acoustics 121 (1999) 468–475.
[10] L. Brillouin, Wave Propagation in Periodic Structures, Dover Publications, New York, 1946.
[11] W. O'Connor, D. Lang, Control Position control of flexible robot arms using mechanical waves, American Society of Mechanical Engineers, Journal of Dynamic System Measurement 120 (1998) 334–339.
[12] M. Saigo, N. Tanaka, K. Tani, An approach to vibration control of multiple-pendulum system by wave absorption, American Society of Mechanical Engineers, Journal of Vibration and Acoustics 120 (1998) 524–533.
[13] M. Saigo, H. Usui, A. Koumura, K. Tani, Vibration control of a traveling suspended system by wave absorbing control, Transactions of the Japan Society of Mechanical Engineers 65–632 (1999) 1434–1440 (in Japanese).